Microscopic analysis of relaxation mechanisms from energy- and time-resolved two-photon photoemission spectra of metal surfaces

2005 J. Phys.: Condens. Matter 17 S245

(http://iopscience.iop.org/0953-8984/17/8/004)

INSTITUTE OF PHYSICS PUBLISHING JOURNAL OF PHYSICS: CONDENSED MATTER

J. Phys.: Condens. Matter **17** (2005) S245–S259 doi:10.1088/0953-8984/17/8/004

Microscopic analysis of relaxation mechanisms from energy- and time-resolved two-photon photoemission spectra of metal surfaces

Mamoru Sakaue

Nanotechnology Research Centre, Fujitsu Laboratories Ltd, 10-1 Morinosato-Wakamiya, Atsugi, Kanagawa 243-0197, Japan

Received 4 January 2005, in final form 4 January 2005
Published 11 February 2005
Online at stacks.iop.org/JPhysCM/17/S245

Abstract

Microscopic theory of energy- and time-resolved (ER- and TR-) two-photon photoemission (2PPE) from metal surfaces is presented from the viewpoint of many-body dynamics of the electron system. The effects of hole dynamics in the occupied states at the surfaces are investigated by the nonequilibrium Green function method. In the macroscopic theory based on the density matrix method, it is usually considered that dephasing is due to elastic scattering and energy relaxation is due to inelastic scattering; however, it is demonstrated that inelastic electron–electron scattering of the photoexcited holes from the occupied states to the bulk can account for both dephasing and acceleration of energy relaxation. On the basis of analytical and numerical analyses for ER- and TR-2PPE on Cu(111), the relations of the macroscopic relaxation times with the electron and hole lifetimes are clarified.

1. Introduction

Recently, as well as the energetic structures, the dynamical properties of solid surfaces are attracting interest from researchers in chemistry and optics. By means of two-photon photoemission (2PPE) spectroscopy using ultraviolet and visible light, we can obtain information on the properties of electrons and holes in occupied and unoccupied states from several electron volts below the Fermi energy (chemical potential) to the vacuum level. Electrons and holes excited by the light survive over femtosecond to picosecond timescales and can cause photochemical reactions and light emission. The timescale of the reactions to the input of light is determined by the rate of scattering of the photoexcited electrons and holes. From a macroscopic viewpoint, the scattering results in energy relaxation, i.e., density decay observed as the relaxation of energy from the partial system of interest to the reservoir, and dephasing, i.e., loss of quantum coherence.

By means of macroscopic analysis based on the density matrix method, we can obtain the energy relaxation time T_1 and the dephasing time T_2. This method was first developed for atomic systems in which, mainly, the energy relaxation occurs due to radiative relaxation, and the dephasing occurs due to atomic collisions [1]. By modifying the explanation of the relaxation mechanisms, this theory can also be applied to solids where interactions involving lattice vibrations as well as electrons and photons can take place, so that the degree of freedom of quasielastic and inelastic scattering becomes large [2]. For example, in semiconductors, the energy relaxation can occur due to cascade processes (inelastic scattering) as well as the radiative relaxation, and the dephasing can occur due to (quasi-) elastic scattering around defects and impurities.

Owing to the recent development of femtosecond laser technology, experiments of 2PPE spectroscopy on metal surfaces, e.g., for Cu, Ag, Pt and Ni [3–11], which have image-potential-induced surface states (image states), have become active [12]. By applying the above macroscopic theory to analysis of the energy- and time-resolved (ER- and TR-) 2PPE spectra [13, 14], T_1 and T_2 can be estimated in the same way as for semiconductors. In the discussion of the results obtained, it is usually assumed that T_1 corresponds to the intrinsic lifetime of the image state and T_2 represents an index of thermal fluctuation or strength of (quasi-) elastic scattering at adsorbates or steps on the surfaces. However, the validity of such treatments is not clear since the available phase space for inelastic electron–electron scattering in metals can be much larger than that for semiconductors, as recognized by the experimental and theoretical studies from the viewpoint of excitation mechanisms [15–23], so that the dominant relaxation mechanisms become fundamentally different from the case for semiconductors.

Then we reconsider the relaxation mechanisms at metals. For this purpose, we give an example of 2PPE from Cu(111) that has been investigated extensively by means of both experiments and theories [3, 13, 18, 20, 24–29]. Cu(111) surfaces have a projected band gap in the surface normal direction, where an occupied surface state (the Shockley state at $\epsilon_q - \epsilon_F = -0.45\,\mathrm{eV}$) and an unoccupied surface state (the $n = 1$ image state at $\epsilon_k - \epsilon_F = 4.1\,\mathrm{eV}$) are located within the gap. Here, ϵ_F denotes the Fermi level. When the pump photon energy $\hbar\omega_{pu}$ is slightly detuned from the resonance $\epsilon_k - \epsilon_q$, the 2PPE energy spectra exhibit two peaks: the SS peak at $\epsilon_q + \hbar\omega_{pu} + \hbar\omega_{pr}$ and the IS peak at $\epsilon_k + \hbar\omega_{pr}$, where $\hbar\omega_{pr}$ denotes the probe photon energy. The SS peak occurs due to the direct two-photon process in which the excitation by the pump photon is immediately followed by the excitation by the probe photon via a virtual intermediate state. Meanwhile, it is considered that the IS peak occurs due to scattering which results in dephasing [3, 13, 14].

Macroscopically, 2PPE from this system can be described by a three-level model based on the density matrix method. Usually, an initial state $|0\rangle$, an intermediate state $|1\rangle$ and a final state $|2\rangle$ are introduced (see figure 1(a)), where $|2\rangle$ has an infinite lifetime and T_1 and T_2 are given for the two-level system consisting of $|0\rangle$ and $|1\rangle$ (it is noted that extended versions of this model can be introduced by assuming the dephasing times between $|2\rangle$ and the other states). It is known that the simulations by this model can reproduce the experimental pump–probe correlation traces (photoelectron intensities as functions of the pump–probe delay time), choosing T_1 and T_2 as free parameters [3], although the physical meanings of the parameters are still unclear.

From a microscopic viewpoint, the pump laser excites a hole in the occupied surface state $|q\rangle$ and an electron in the unoccupied state $|k\rangle$ (see figure 1(b)). Then the electron in $|k\rangle$ can be inelastically scattered due to interactions with the electron system in the bulk so that $|k\rangle$ has a finite lifetime τ_k. It is usually assumed that the density of $|k\rangle$ decreases until the excitation by the probe laser to the free electron state $|f\rangle$ above the vacuum level occurs so that $\tau_k = T_1$ is

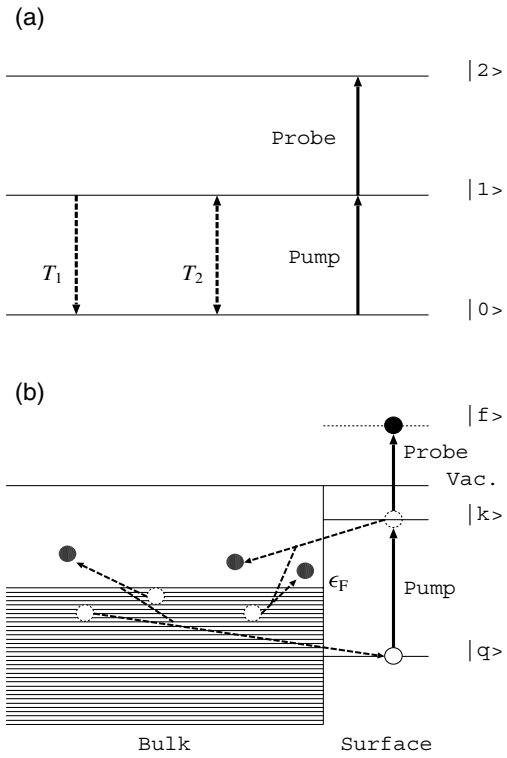

Figure 1. (a) The three-level model of 2PPE used in the macroscopic theory. $|0\rangle$, $|1\rangle$ and $|2\rangle$ denote the initial, intermediate and final states. The energy relaxation T_1 and the dephasing T_2 are introduced between $|0\rangle$ and $|1\rangle$. (b) A schematic diagram of a microscopic model of 2PPE from metal surfaces considering the inelastic electron–electron scattering involving an occupied state $|q\rangle$ and an unoccupied state $|k\rangle$. $|f\rangle$ denotes a free electron state above the vacuum level.

measured as the decay time of the pump–probe correlation trace. Then quantitative analyses of T_1 were attempted by the direct comparison between the experimental T_1 and the theoretical τ_k, as the inverse of the imaginary part of the self-energies of the unoccupied electron states [7].

However the analysis of T_2 has been limited to being qualitative. Meanwhile, in the same way as the electron in $|k\rangle$, the hole in $|q\rangle$ will decay due to inelastic scattering so that $|q\rangle$ has a finite lifetime τ_q although its effect on the relaxation has not been discussed in the usual analyses. The hole decay accompanies excitation of secondary electrons and holes, and hence will result in electron thermalization which causes dephasing by repeating the scattering. In order to clarify the relations between the hole decay and the dephasing, the author and co-workers have investigated the TR- and ER-2PPE spectra of metal surfaces by means of many-body theories based on the nonequilibrium Green function method [24–26, 30]. In the studies, it has been shown in time and energy domains, respectively, that as well as the dephasing the hole scattering can account for the energy transfer between the surface and the bulk so that the energy relaxation of the 'two-level system' consisting of $|q\rangle$ and $|k\rangle$ is accelerated.

In this paper, summarizing the results from the TR- and ER-2PPE spectra, the relations of $T_1 = \hbar/2\Gamma_1$ and $T_2 = \hbar/\Gamma_2$ with $\tau_k = \hbar/2\gamma_k$ and $\tau_q = \hbar/2\gamma_q$ are investigated in detail. By analysing the spectral widths in the energy spectra for continuous light as functions of $\hbar\omega$ ($=\hbar\omega_{\rm pu} = \hbar\omega_{\rm pr}$), it is shown that Γ_1 depends on $\hbar\omega$ whereas $\Gamma_2 = \gamma_q$ is independent of

$\hbar\omega$. Meanwhile, in the femtosecond TR spectra for $\hbar\omega_{\rm pu} = \epsilon_k - \epsilon_q - 0.1$ eV, it is shown that $T_1 \sim [\tau_k^{-1} + \tau_q^{-1}]^{-1}$ and $T_2 \sim \tau_q$. Referring to the analytical results, the above differences between the analyses in time and energy domains are discussed.

2. Theory

The model electron system is described by a Hamiltonian $H_0 + V$, where the unperturbed Hamiltonian is given by

$$H_0 = \epsilon_q c_q^\dagger c_q + \epsilon_k c_k^\dagger c_k + \sum_f \epsilon_f c_f^\dagger c_f + \sum_p \epsilon_p c_p^\dagger c_p, \tag{2.1}$$

and the Coulomb interactions between electrons by

$$V = \tfrac{1}{2} \sum_{\kappa,\lambda,\mu,\nu} V_{\kappa\lambda/\mu\nu} c_\lambda^\dagger c_\kappa^\dagger c_\mu c_\nu \qquad (\kappa, \lambda, \mu, \nu = q, k, f, p). \tag{2.2}$$

Here E, $c^\dagger$ and c denote the energy and the creation and annihilation operators, respectively, for the states given by the indices, where p denotes a bulk state and the others are the same as those defined in section 1. For simplicity, the degree of freedom of the spin is implied in the indices of the electron states. By introducing the interactions of an electron with the laser pulses,

$$W(t) = \sum_f W_{fk}(t) c_f^\dagger c_k + W_{kq}(t) c_k^\dagger c_q + \text{H.c.}, \tag{2.3}$$

the photoelectron density $\rho_{ff}(t)$ is obtained by solving the Liouville equation,

$$\mathrm{i}\hbar \frac{\partial \rho(t)}{\partial t} = [H_0 + V + W(t), \rho(t)], \tag{2.4}$$

where $\rho(t)$ denotes the density matrix in the Schrödinger representation.

By expanding with respect to $V + W(t)$, $\rho_{ff}(t)$ is obtained as a sum of multiple integrals of many-body correlation functions [31]. Then, by expanding the correlation functions into products of one-body functions, we obtain

$$\begin{aligned}\rho_{ff}(t_{\rm ob}) = -\mathrm{i}\hbar \int_\infty^{-\infty} \mathrm{d}t_1' \int_\infty^{-\infty} \mathrm{d}t_2' \int_{-\infty}^{\infty} \mathrm{d}t_2 \int_{-\infty}^{\infty} \mathrm{d}t_1 \\ \times \theta(t_{\rm ob} - t_2')\theta(t_2' - t_1')\theta(t_{\rm ob} - t_2)\theta(t_2 - t_1) \\ \times W_{qk}(t_1') W_{kf}(t_2') W_{fk}(t_2) W_{kq}(t_1) \\ \times G_{ff}^{++}(t_{\rm ob} - t_2) G_{kk}^{++}(t_2 - t_1) \\ \times G_{qq}^{+-}(t_{\rm ob} - t_1, t_1' - t_{\rm ob}) \\ \times G_{kk}^{--}(t_1' - t_2') G_{ff}^{--}(t_2' - t_{\rm ob}),\end{aligned} \tag{2.5}$$

where $t_{\rm ob}$ is the observation time of the photoelectron and $\theta(t)$ is a step function. Here the Vs are renormalized into the nonequilibrium Green functions defined by a (2×2) matrix [25],

$$\mathbf{G}(t, t'; t_{\rm ob}) = \begin{pmatrix} G^{++}(t, t'; t_{\rm ob}) & G^{+-}(t, t'; t_{\rm ob}) \\ G^{-+}(t, t'; t_{\rm ob}) & G^{--}(t, t'; t_{\rm ob}) \end{pmatrix}. \tag{2.6}$$

G^{++} and G^{--} are causal and anti-causal Green functions, respectively, that satisfy $G_{\mu\nu}^{++}(t, t'; t_{\rm ob}) = [G_{\nu\mu}^{--}(t', t; t_{\rm ob})]^*$, for which the $t_{\rm ob}$ dependence is usually negligible so that G^{++} and G^{--} can be expressed as functions of $t - t'$. Assuming a constant decay rate represented by a lifetime $\tau_k = \hbar/2\gamma_k$, $G_{kk}^{++}(t - t')$ is given by

$$\begin{aligned}G_{kk}^{++}(t - t') = (\mathrm{i}\hbar)^{-1}\{[1 - f(\epsilon_k)]\theta(t - t')\mathrm{e}^{(-\mathrm{i}\epsilon_k - \gamma_k)(t - t')/\hbar} \\ - f(\epsilon_k)\theta(t' - t)\mathrm{e}^{(\mathrm{i}\epsilon_k - \gamma_k)(t' - t)/\hbar}\},\end{aligned} \tag{2.7}$$

where $f(E)$ denotes the Fermi distribution function. For simplicity, it is assumed that the energy shift due to the scattering is implied in ϵ_k. The decay of $G^{++}_{ff}(t-t')$ is assumed to be negligible since the photoelectrons will be excited outside the surface and leave the surface immediately so that no scattering with the bulk electrons can occur.

$G^{+-}(t,t';t_{\rm ob}) = G^{+-}(t_{\rm ob}-t, t'-t_{\rm ob})$ is an interbranch function in which t and t' give the times in the forward and backward branches, respectively, of the Keldysh contour [25]. The lowest order term of G^{+-}_{qq} is given by

$$\begin{aligned} G^{+-\,[1]}_{qq}(t_{\rm ob}-t, t'-t_{\rm ob}) &= -{\rm i}\hbar\theta(t_{\rm ob}-t)\theta(t_{\rm ob}-t')G^{++}_{qq}(t-t_{\rm ob})G^{--}_{qq}(t_{\rm ob}-t') \\ &= -({\rm i}\hbar)^{-1}[f(\epsilon_q)]^2\theta(t_{\rm ob}-t)\theta(t_{\rm ob}-t') \\ &\quad\times {\rm e}^{({\rm i}\epsilon_q-\gamma_q)(t_{\rm ob}-t)/\hbar}{\rm e}^{(-{\rm i}\epsilon_q-\gamma_q)(t_{\rm ob}-t')/\hbar}. \end{aligned} \tag{2.8}$$

For $t=t'$, this term represents the decay of the hole density in $|q\rangle$ due to the inelastic scattering after an instantaneous excitation at t:

$$|G^{+-\,[1]}_{qq}(t_{\rm ob}-t, t-t_{\rm ob})| = \hbar^{-1}[f(\epsilon_q)]^2\theta(t_{\rm ob}-t){\rm e}^{-(t_{\rm ob}-t)/\tau_q}. \tag{2.9}$$

Then, for $W_{fk}(t)\propto\delta(t-t_{\rm d})$ and $W_{kq}(t)\propto\delta(t)$, we obtain the photoelectron density as [24]

$$\rho^{[1]}_{ff}(t_{\rm ob};t_{\rm d}) \propto \theta(t_{\rm d}){\rm e}^{-t_{\rm d}/\tau_k}\theta(t_{\rm ob}-t_{\rm d}){\rm e}^{-t_{\rm ob}/\tau_q}. \tag{2.10}$$

Here, $\delta(t)$ denotes the δ function and $t_{\rm d}$ the pump–probe delay time. This shows that the most electrons are photoemitted within the time from $t=t_{\rm d}$ to $t_{\rm d}+\tau_q$, where $t=0$ is the time of the excitation by the pump, and at large $t_{\rm ob}$ the probability of photoemission becomes small because of the loss of coherence due to the hole decay. Assuming that the measured photoelectron intensity $I_f(t_{\rm d})$ is proportional to the integral of $\rho_{ff}(t_{\rm ob};t_{\rm d})$ over $t_{\rm ob}$, the lowest order term of $I_f(t_{\rm d})$ is obtained as

$$\begin{aligned} I^{[1]}_f(t_{\rm d}) &\propto \int_{-\infty}^{\infty}{\rm d}t_{\rm ob}\,\rho^{[1]}_{ff}(t_{\rm ob};t_{\rm d}) \\ &\propto \theta(t_{\rm d})\exp[-t_{\rm d}(\tau_k^{-1}+\tau_q^{-1})]. \end{aligned} \tag{2.11}$$

This shows that the energy dissipation from the surface to the bulk due to the decay of a polarization consisting of the electron in $|k\rangle$ and the hole in $|q\rangle$ accounts for the macroscopic energy relaxation, so that the lifetime of the intermediate state of the 2PPE process corresponds to the lifetime of the polarization rather than τ_k.

The inelastic hole scattering can result in the excitation of secondary electrons and holes in the bulk expressed by the higher order terms of $G^{+-}(t_{\rm ob}-t, t'-t_{\rm ob})$ with respect to V; for example, the second-order term is given by [25]

$$\begin{aligned} G^{+-\,[2]}_{qq}(t_{\rm ob}-t, t'-t_{\rm ob}) &= -({\rm i}\hbar)^{-1}[f(\epsilon_q)]^2\theta(t_{\rm ob}-t)\theta(t_{\rm ob}-t') \\ &\quad\times\sum_{\kappa}\sum_{\mu}\sum_{\nu}[1-f(\epsilon_\kappa)]f(\epsilon_\mu)f(\epsilon_\nu)[V_{\mu\nu/q\kappa}V_{\kappa q/\nu\mu}-V_{\mu\nu/q\kappa}V_{\kappa q/\mu\nu}] \\ &\quad\times[(\epsilon_q+\epsilon_\kappa-\epsilon_\mu-\epsilon_\nu)^2+(\gamma_q-\gamma_\kappa-\gamma_\mu-\gamma_\nu)^2]^{-1} \\ &\quad\times\{{\rm e}^{({\rm i}\epsilon_q-\gamma_q)(t_{\rm ob}-t)/\hbar}-{\rm e}^{[{\rm i}(\epsilon_\kappa-\epsilon_\mu-\epsilon_\nu)-(\gamma_\kappa+\gamma_\mu+\gamma_\nu)](t_{\rm ob}-t)/\hbar}\} \\ &\quad\times\{{\rm e}^{(-{\rm i}\epsilon_q-\gamma_q)(t_{\rm ob}-t')/\hbar}-{\rm e}^{[-{\rm i}(\epsilon_\kappa-\epsilon_\mu-\epsilon_\nu)-(\gamma_\kappa+\gamma_\mu+\gamma_\nu)](t_{\rm ob}-t')/\hbar}\}, \end{aligned} \tag{2.12}$$

where κ in the summation is an index for the secondary electron, and μ and ν are for the secondary holes. The effects of the second-order processes are discussed in the following sections.

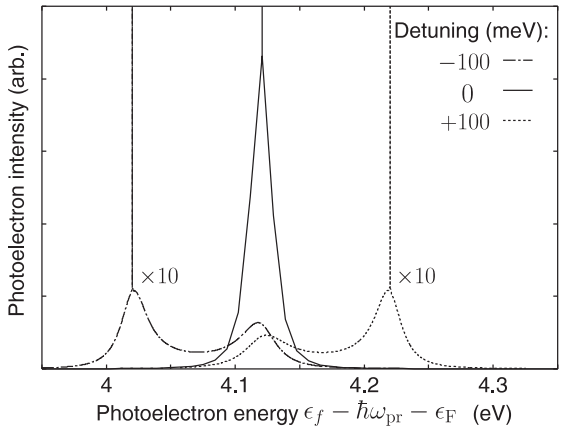

Figure 2. 2PPE energy spectra of Cu(111) obtained from the microscopic theory.

3. Energy spectra

Giving $W_{\mu\nu}(t) = [W_{\nu\mu}(t)]^* = W_{\mu\nu}\exp(-\mathrm{i}\omega t)$, the form of the 2PPE energy spectrum for single-colour continuous light [26] is obtained as

$$
\begin{aligned}
I[\epsilon_f] \propto \rho_{ff} = {} & |W_{fk}W_{kq}|^2[(\epsilon_f-\epsilon_q-2\hbar\omega)^2+\gamma_q^2]^{-1}[(\epsilon_k-\epsilon_q-\hbar\omega)^2+(\gamma_k+\gamma_q)^2]^{-1} \\
& \times \Bigg\{1+\sum_\kappa\sum_\mu\sum_\nu[1-f(\epsilon_\kappa)]f(\epsilon_\mu)f(\epsilon_\nu)[V_{\mu\nu/q\kappa}V_{\kappa q/\nu\mu}-V_{\mu\nu/q\kappa}V_{\kappa q/\mu\nu}] \\
& \times \frac{1}{(\epsilon_f+\epsilon_\kappa-\epsilon_\mu-\epsilon_\nu-2\hbar\omega)^2+(\gamma_\kappa+\gamma_\mu+\gamma_\nu)^2} \\
& \times \frac{1}{(\epsilon_k+\epsilon_\kappa-\epsilon_\mu-\epsilon_\nu-\hbar\omega)^2+(\gamma_k+\gamma_\kappa+\gamma_\mu+\gamma_\nu)^2} \\
& \times |(\epsilon_f-2\hbar\omega)+(\epsilon_k-\hbar\omega-\mathrm{i}\gamma_k)+(-\epsilon_q-\mathrm{i}\gamma_q) \\
& +[\epsilon_\kappa-\epsilon_\mu-\epsilon_\nu-\mathrm{i}(\gamma_\kappa+\gamma_\mu+\gamma_\nu)]|^2\Bigg\}. \qquad (3.1)
\end{aligned}
$$

The first term in the braces accounts for the SS peak (identical to the 2ω peak in the single-colour 2PPE) due to a process where first an electron in $|q\rangle$ is photoexcited to $|k\rangle$ virtually and subsequently it is photoexcited to $|f\rangle$. The second term accounts for the IS (1ω) peak due to processes where, after the virtual electron photoexcitation from $|q\rangle$ to $|k\rangle$, the hole in $|q\rangle$ is scattered inelastically by the bulk electrons and subsequently the electron in $|k\rangle$ is photoexcited to $|f\rangle$.

Figure 2 shows the 2PPE spectra of Cu(111) for -100, 0 and +100 meV detunings. The energy levels and lifetimes of $|q\rangle$ and $|k\rangle$ are given as parameters from the literature on theoretical work: $\epsilon_q-\epsilon_{\rm F}=-0.445$ eV and $\tau_q=26$ fs ($\gamma_q=12.7$ meV) for the Shockley state [27] and $\epsilon_k-\epsilon_{\rm F}=4.12$ eV and $\tau_k=23$ fs ($\gamma_k=14.3$ meV) for the image state [28]. The lifetime of a bulk electron in $|p\rangle$ is given as 30 fs for $|\epsilon_p-\epsilon_{\rm F}|=1$ eV [29] within the Fermi liquid theory [32]. Here a flat density of states for the bulk electrons is assumed. For simplicity, $V_{\mu\nu/q\kappa}V_{\kappa q/\nu\mu}-V_{\mu\nu/q\kappa}V_{\kappa q/\mu\nu}$ in (2.12) and (3.1) is assumed to be a constant value which gives $\gamma_q=12.7$ meV by calculation of the self-energy within the second order with respect to V.

For ±100 meV detunings, the peak at 4.12 eV is attributable to the IS peak and the peak at 4.12 ± 0.10 eV to the SS peak. The occurrence of the IS peak is due to the energy

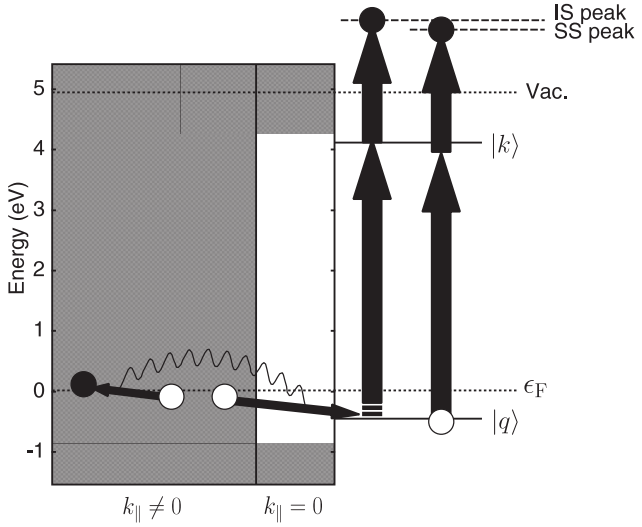

Figure 3. A schematic diagram of the 2PPE processes accounting for the SS and IS peaks at Cu(111). $k_\parallel$ denotes the parallel component of the wavevector with respect to the surface. The shaded area shows the continuum. The thick vertical arrows denote the photoexcitation by the pump and probe laser. The pump energy is slightly smaller than the resonance $\epsilon_k - \epsilon_q$ (the broken part of the thick arrow denotes the detuning). The thin arrows connected with a wave denote the inelastic electron–electron scattering.

transfer between the surface and the bulk accompanying the inelastic scattering of the hole (see figure 3). Macroscopically, this effect is explained by the quasielastic scattering of the virtual polarization at the surface consisting of the electron in $|k\rangle$ and the hole in $|q\rangle$ into a real polarization consisting of the electron in $|k\rangle$ and the secondary electrons and holes in the bulk. For 0 detuning, the processes accounting for the two peaks interfere with each other, and a strong peak is observed at 4.12 eV. The two-peak structure agrees with the experiments [4, 11] except for the sharp structure on the SS peak. This structure is due to the excitation of the secondary electrons and holes with infinitesimal excitation energies accompanied by the quasielastic hole transfer from the surface to the bulk, i.e., a sort of Fermi surface effect. Thus the structure may vanish when the higher order terms are renormalized into G_{qq}^{+-} [2]. This problem will be an important future subject.

From macroscopic theory, the form of the 2PPE spectra was obtained as [26]

$$I^{\mathrm{macro}}[\epsilon_2] \propto \rho_{22}^{\mathrm{macro}} \propto \frac{1}{(\epsilon_2 - \epsilon_0 - 2\hbar\omega)^2 + \Gamma_2^2} \frac{1}{(\epsilon_2 - \epsilon_1 - \hbar\omega)^2 + \Gamma_1^2}, \tag{3.2}$$

where $\Gamma_1 = \hbar/2T_1$ and $\Gamma_2 = \hbar/T_2$. It is clear that this equation shows the two-peak structure in the same way as the microscopic theory. On comparing this with (3.1), the relation $\Gamma_2 = \gamma_q$ at the SS peak is immediately understood whereas the relation of Γ_1 with γ_k and γ_q is not clear yet.

In order to clarify the relations of Γ_1 and Γ_2 with γ_k and γ_q in detail, numerical analyses of the spectral widths are made. A sum of two Lorentzians is fitted to each spectrum by the least squares method so that the widths of the IS and SS peak structures are obtained [26]. Figure 4 shows the results for -400 meV $< \Delta E <$ +400 meV with the results from macroscopic theory for $\Gamma_1 = \gamma_k$ and $\Gamma_2 = \gamma_q$. Here, $\Delta E = \hbar\omega - (\epsilon_k - \epsilon_q)$ denotes the detuning of the pump energy from the resonance. The widths of the SS peak structure agree extremely well between the microscopic and macroscopic theories. The effect of interference [33] between

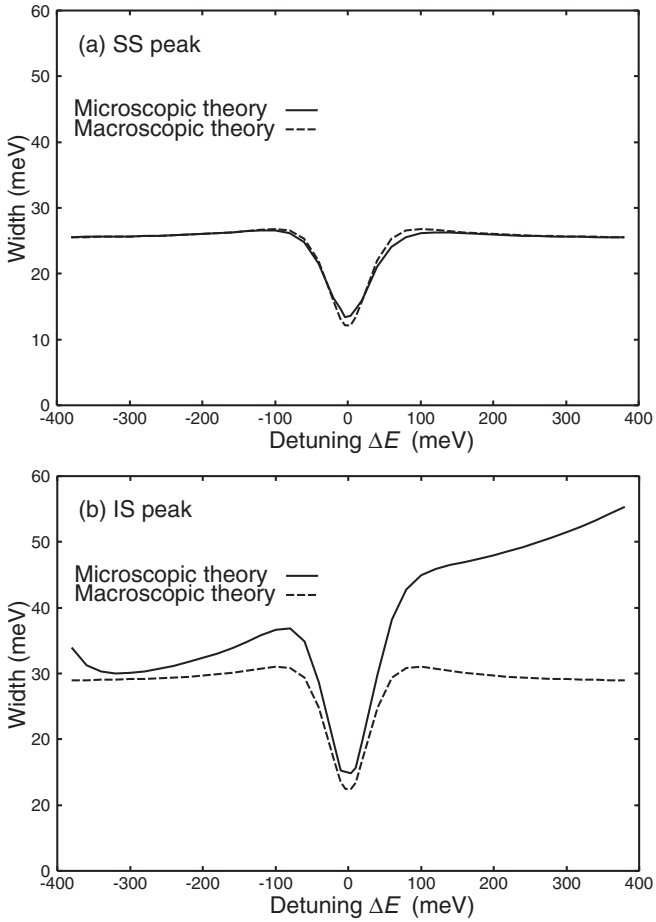

Figure 4. Energy widths of (a) the SS peak and (b) the IS peak structures in the 2PPE spectrum of Cu(111) as functions of the detuning $\Delta E = \hbar\omega - (\epsilon_k - \epsilon_q)$. The solid curves show the results from the microscopic theory. The dashed curves show the results from the macroscopic theory for $\Gamma_1 = \gamma_k$ and $\Gamma_2 = \gamma_q$.

the processes accounting for the SS and IS peaks is manifested in the dip structure in the vicinity of the resonance in which the two processes enhance with each other so that the peak structures in the spectra become narrow. The energy width of the SS peak structure converges to $2\Gamma_2 = 2\gamma_q = 25.4$ meV for large detuning. This result clearly demonstrates the correspondence between the hole decay and the dephasing.

Qualitatively, in the same way as the SS peak, the energy width of the IS peak structure becomes narrow in the vicinity of the resonance due to the interference effect. However, contrary to the SS peak case, the energy width is quantitatively different for the microscopic and macroscopic theories. In the macroscopic theory, the width converges to $2\Gamma_1 = 2\gamma_k = 28.6$ meV for large detuning. Meanwhile, in the microscopic theory, the width is close to $2\gamma_k$ for $\Delta E = \epsilon_q - \epsilon_F = -0.45$ eV, and increases for large ΔE so that the peak structure undergoes a collapse accompanied by the decrease of the peak height (13% of the SS peak for $\Delta E = 400$ meV). Here, the increase of the width for $\Delta E < -300$ meV is due to the collapse of the peak structure in the vicinity of the Fermi cut-off. Ignoring the region near the

resonance, the difference in width between the two theories is approximately proportional to $[\hbar\omega - (\epsilon_k - \epsilon_F)]^2 = [\Delta E + (\epsilon_F - \epsilon_q)]^2$, i.e., the available phase space for the hole scattering. This means that Γ_1 is obtained as a function of ΔE when fitting the macroscopic theory to the results from the microscopic theory for each ΔE, giving Γ_1 and Γ_2 as free parameters. The measurement of the widths of the peak structures as functions of ΔE has been attempted [34]; however, it will be an issue for the future to accumulate sufficient high resolution experimental spectra to compare with figure 4.

4. Time-resolved spectra

In order to obtain the TR-2PPE spectra, the matrix elements of W are given by

$$W_{kq}(t) = -M_{kq}\mathcal{E}(t)\mathrm{e}^{-\mathrm{i}\omega_{\mathrm{pu}}t} \tag{4.1}$$

and

$$W_{fk}(t; t_\mathrm{d}) = -M_{fk}\mathcal{E}(t - t_\mathrm{d})\mathrm{e}^{-\mathrm{i}\omega_{\mathrm{pr}}t}, \tag{4.2}$$

where $\mathcal{E}(t)$ is the pulse envelope function. Giving $\mathcal{E}(t) = \bar{\mathcal{E}}\theta(t)\exp(-\gamma_\Delta t/2\hbar)$, the analytical form of the photoelectron intensity is obtained as

$$\begin{aligned} I(t_\mathrm{d}) &\propto \int_{-\infty}^{\infty} \mathrm{d}t\, \rho_{ff}(t; t_\mathrm{d}) \\ &= |M_{fk}M_{kq}|^2|\bar{\mathcal{E}}|^4[\hat{I}^{[1]}(t_\mathrm{d}) + \hat{I}^{[2]}(t_\mathrm{d})], \end{aligned} \tag{4.3}$$

where

$$\begin{aligned} \hat{I}^{[1]}(t_\mathrm{d}) &= \int_{-\infty}^{\infty} \mathrm{d}t\, \rho_{ff}^{[1]}(t; t_\mathrm{d}) \\ &= a_1^{[1]}[\theta(t_\mathrm{d})\mathrm{e}^{-2(\gamma_k+\gamma_q)t_\mathrm{d}/\hbar} + \theta(-t_\mathrm{d})\mathrm{e}^{\gamma_\Delta t_\mathrm{d}/\hbar}] \\ &\quad + 2\,\mathrm{Im}\Big[a_2^{[1]}\{\theta(t_\mathrm{d})\mathrm{e}^{[\mathrm{i}(\epsilon_k-\epsilon_q-\hbar\omega_{\mathrm{pu}})-(\gamma_k+\gamma_q)-\gamma_\Delta/2]t_\mathrm{d}/\hbar} + \theta(-t_\mathrm{d})\mathrm{e}^{\gamma_\Delta t_\mathrm{d}/\hbar}\}\Big] \\ &\quad + a_3^{[1]}[\theta(t_\mathrm{d})\mathrm{e}^{-\gamma_\Delta t_\mathrm{d}/\hbar} + \theta(-t_\mathrm{d})\mathrm{e}^{\gamma_\Delta t_\mathrm{d}/\hbar}], \end{aligned} \tag{4.4}$$

$$\begin{aligned} \hat{I}^{[2]}(t_\mathrm{d}) &= \int_{-\infty}^{\infty} \mathrm{d}t\, \rho_{ff}^{[2]}(t; t_\mathrm{d}) \\ &= \sum_\kappa \sum_\mu \sum_\nu [1 - f(\epsilon_\kappa)]f(\epsilon_\mu)f(\epsilon_\nu)[V_{\mu\nu/q\kappa}V_{\kappa q/\nu\mu} - V_{\mu\nu/q\kappa}V_{\kappa q/\mu\nu}] \\ &\quad \times [(\epsilon_q + \epsilon_\kappa - \epsilon_\mu - \epsilon_\nu)^2 + (\gamma_q - \gamma_\kappa - \gamma_\mu - \gamma_\nu)^2]^{-1} \\ &\quad \times F(\epsilon_\kappa - \epsilon_\mu - \epsilon_\nu, \gamma_\kappa + \gamma_\mu + \gamma_\nu; t_\mathrm{d}), \end{aligned} \tag{4.5}$$

$$\begin{aligned} F(\epsilon, \gamma; t_\mathrm{d}) &= a_1^{[2]}(\epsilon_q, \gamma_q)\Big[\theta(t_\mathrm{d})\mathrm{e}^{-2(\gamma_k+\gamma_q)t_\mathrm{d}/\hbar} + \theta(-t_\mathrm{d})\mathrm{e}^{\gamma_\Delta t_\mathrm{d}/\hbar}\Big] \\ &\quad + a_1^{[2]}(\epsilon, \gamma)\Big[\theta(t_\mathrm{d})\mathrm{e}^{-2(\gamma_k+\gamma)t_\mathrm{d}/\hbar} + \theta(-t_\mathrm{d})\mathrm{e}^{\gamma_\Delta t_\mathrm{d}/\hbar}\Big] + 2\,\mathrm{Im}\Big[a_2^{[2]}(\epsilon_q, \epsilon, \gamma_q, \gamma) \\ &\quad \times \Big[\theta(t_\mathrm{d})\mathrm{e}^{[\mathrm{i}(\epsilon_k-\epsilon_q-\hbar\omega_{\mathrm{pu}})-(\gamma_k+\gamma_q+\gamma_\Delta/2)]t_\mathrm{d}/\hbar} + \theta(-t_\mathrm{d})\mathrm{e}^{\gamma_\Delta t_\mathrm{d}/\hbar}\Big] \\ &\quad + a_2^{[2]}(\epsilon, \epsilon_q, \gamma, \gamma_q)\Big[\theta(t_\mathrm{d})\mathrm{e}^{[\mathrm{i}(\epsilon_k-\epsilon-\hbar\omega_{\mathrm{pu}})-(\gamma_k+\gamma+\gamma_\Delta/2)]t_\mathrm{d}/\hbar} + \theta(-t_\mathrm{d})\mathrm{e}^{\gamma_\Delta t_\mathrm{d}/\hbar}\Big] \\ &\quad + a_3^{[2]}(\epsilon_q, \epsilon, \gamma_q, \gamma)\Big[\theta(t_\mathrm{d})\mathrm{e}^{[\mathrm{i}(\epsilon_q-\epsilon)-(2\gamma_k+\gamma_q+\gamma)]t_\mathrm{d}/\hbar} + \theta(-t_\mathrm{d})\mathrm{e}^{\gamma_\Delta t_\mathrm{d}/\hbar}\Big]\Big] \\ &\quad + \Big[a_4^{[2]}(\epsilon_q, \gamma_q) + a_4^{[2]}(\epsilon, \gamma) + a_5^{[2]}(\epsilon_q, \epsilon, \gamma_q, \gamma)\Big] \\ &\quad \times \Big[\theta(t_\mathrm{d})\mathrm{e}^{-\gamma_\Delta t_\mathrm{d}/\hbar} + \theta(-t_\mathrm{d})\mathrm{e}^{\gamma_\Delta t_\mathrm{d}/\hbar}\Big], \end{aligned} \tag{4.6}$$

$$a_1^{[1]} = \frac{\hbar^2}{(\epsilon_f - \epsilon_k - \hbar\omega_{\rm pr})^2 + (\gamma_k + \gamma_\Delta/2)^2} \times \left[\frac{\hbar}{2\gamma_q} - \frac{\hbar(2\gamma_k + 4\gamma_q + \gamma_\Delta)}{(\epsilon_f - \epsilon_k - \hbar\omega_{\rm pr})^2 + (\gamma_k + \gamma_\Delta/2 + 2\gamma_q)^2} + \frac{\hbar}{2(\gamma_k + \gamma_q + \gamma_\Delta)} \right], \quad (4.7)$$

$$a_2^{[1]} = \frac{\hbar}{\epsilon_f - \epsilon_k - \hbar\omega_{\rm pr} - {\rm i}(\gamma_k + \gamma_\Delta/2)} \frac{\hbar}{\epsilon_f - \epsilon_q - \hbar\omega_{\rm pu} - \hbar\omega_{\rm pr} - {\rm i}(\gamma_q - \gamma_\Delta)} \times \left[\frac{\hbar}{{\rm i}2\gamma_q} - \frac{\hbar}{\epsilon_f - \epsilon_q - \hbar\omega_{\rm pu} - \hbar\omega_{\rm pr} + {\rm i}(\gamma_q + \gamma_\Delta)} + \frac{\hbar}{\epsilon_f - \epsilon_k - \hbar\omega_{\rm pr} - {\rm i}(\gamma_k + \gamma_\Delta/2 + 2\gamma_q)} + \frac{\hbar}{\epsilon_k - \epsilon_q - \hbar\omega_{\rm pu} + {\rm i}(\gamma_k + \gamma_q + 3\gamma_\Delta/2)} \right], \quad (4.8)$$

$$a_3^{[1]} = \frac{\hbar^2}{(\epsilon_f - \epsilon_q - \hbar\omega_{\rm pu} - \hbar\omega_{\rm pr})^2 + (\gamma_q - \gamma_\Delta)^2} \times \left[\frac{\hbar}{2\gamma_q} - \frac{2\hbar(\gamma_q + \gamma_\Delta)}{(\epsilon_f - \epsilon_q - \hbar\omega_{\rm pu} - \hbar\omega_{\rm pr})^2 + (\gamma_q + \gamma_\Delta)^2} + \frac{\hbar}{2\gamma_\Delta} \right], \quad (4.9)$$

$$a_1^{[2]}(\epsilon, \gamma) = \frac{\hbar^2}{(\epsilon_k - \epsilon - \hbar\omega_{\rm pu})^2 + (\gamma_k + \gamma - \gamma_\Delta/2)^2} \frac{\hbar^2}{(\epsilon_f - \epsilon_k - \hbar\omega_{\rm pr})^2 + (\gamma_k + \gamma_\Delta/2)^2} \times \left[\frac{\hbar}{2\gamma} - \frac{2\hbar(\gamma_k + 2\gamma + \gamma_\Delta/2)}{(\epsilon_f - \epsilon_k - \hbar\omega_{\rm pr})^2 + (\gamma_k + \gamma_\Delta/2 + 2\gamma)^2} + \frac{\hbar}{2(\gamma_k + \gamma) + \gamma_\Delta} \right], \quad (4.10)$$

$$\begin{aligned} a_2^{[2]}(\epsilon, \epsilon', \gamma, \gamma') = {} & \frac{\hbar}{\epsilon_f - \epsilon_k - \hbar\omega_{\rm pr} - {\rm i}(\gamma_k + \gamma_\Delta/2)} \\ & \times \left\{ \frac{\hbar^2}{(\epsilon_k - \epsilon - \hbar\omega_{\rm pu})^2 + (\gamma_k + \gamma - \gamma_\Delta/2)^2} \frac{\hbar}{\epsilon_f - \epsilon - \hbar\omega_{\rm pu} - \hbar\omega_{\rm pr} - {\rm i}(\gamma - \gamma_\Delta)} \right. \\ & \times \left[\frac{\hbar}{{\rm i}2\gamma} - \frac{\hbar}{\epsilon_f - \epsilon - \hbar\omega_{\rm pu} - \hbar\omega_{\rm pr} - {\rm i}(\gamma + \gamma_\Delta)} \right. \\ & \left. + \frac{\hbar}{\epsilon_f - \epsilon_k - \hbar\omega_{\rm pr} - {\rm i}(\gamma_k + \gamma_\Delta/2 + 2\gamma)} + \frac{\hbar}{\epsilon_k - \epsilon - \hbar\omega_{\rm pu} + {\rm i}(\gamma_k + \gamma + 3\epsilon_\Delta/2)} \right] \\ & - \frac{\hbar}{\epsilon_k - \epsilon - \hbar\omega_{\rm pu} + {\rm i}(\gamma_k + \gamma - \gamma_\Delta/2)} \frac{\hbar}{\epsilon_k - \epsilon' - \hbar\omega_{\rm pu} - {\rm i}(\gamma_k + \gamma' - \gamma_\Delta/2)} \\ & \times \frac{\hbar}{\epsilon_f - \epsilon' - \hbar\omega_{\rm pu} - \hbar\omega_{\rm pr} - {\rm i}(\gamma' - \gamma_\Delta)} \\ & \times \left[\frac{\hbar}{\epsilon - \epsilon' - {\rm i}(\gamma + \gamma')} - \frac{\hbar}{\epsilon_f - \epsilon_k - \hbar\omega_{\rm pr} + \epsilon - \epsilon' - {\rm i}(\gamma_k + \gamma_\Delta/2 + \gamma + \gamma')} \right. \\ & + \frac{\hbar}{\epsilon_f - \epsilon - \hbar\omega_{\rm pu} - \hbar\omega_{\rm pr} - {\rm i}(\gamma + \gamma_\Delta)} \\ & \left. \left. - \frac{\hbar}{\epsilon_k - \epsilon - \hbar\omega_{\rm pu} + {\rm i}(\gamma_k + \gamma + 3\gamma_\Delta/2)} \right] \right\}, \end{aligned} \quad (4.11)$$

$$a_3^{[2]}(\epsilon, \epsilon', \gamma, \gamma') = [a_3^{[2]}(\epsilon', \epsilon, \gamma', \gamma)]^* = \frac{\hbar}{\epsilon_k - \epsilon - \hbar\omega_{\rm pu} + {\rm i}(\gamma_k + \gamma - \gamma_\Delta/2)} \frac{\hbar}{\epsilon_k - \epsilon' - \hbar\omega_{\rm pu} - {\rm i}(\gamma_k + \gamma' - \gamma_\Delta/2)}$$

$$\times \frac{\hbar^2}{(\epsilon_f-\epsilon_k-\hbar\omega_{\rm pr})^2+(\gamma_k+\gamma_\Delta/2)^2}$$
$$\times\left[\frac{\hbar}{\epsilon-\epsilon'-{\rm i}(\gamma+\gamma')}-\frac{\hbar}{\epsilon_f-\epsilon_k-\hbar\omega_{\rm pr}+\epsilon-\epsilon'-{\rm i}(\gamma_k+\gamma_\Delta/2+\gamma+\gamma')}\right.$$
$$\left.+\frac{\hbar}{\epsilon_f-\epsilon_k-\hbar\omega_{\rm pr}+{\rm i}(\gamma_k+\gamma_\Delta/2+\gamma+\gamma')}+\frac{\hbar}{\epsilon-\epsilon'-{\rm i}(2\gamma_k+\gamma_\Delta+\gamma+\gamma')}\right], \tag{4.12}$$

$$a_4^{[2]}(\epsilon,\gamma)$$
$$=\frac{\hbar^2}{(\epsilon_k-\epsilon-\hbar\omega_{\rm pu})^2+(\gamma_k+\gamma-\gamma_\Delta/2)^2}\frac{\hbar^2}{(\epsilon_f-\epsilon-\hbar\omega_{\rm pu}-\hbar\omega_{\rm pr})^2+(\gamma-\gamma_\Delta)^2}$$
$$\times\left[\frac{\hbar}{2\gamma}-\frac{2\hbar(\gamma+\gamma_\Delta)}{(\epsilon_f-\epsilon-\hbar\omega_{\rm pu}-\hbar\omega_{\rm pr})^2+(\gamma+\gamma_\Delta)^2}+\frac{\hbar}{2\gamma_\Delta}\right], \tag{4.13}$$

$$a_5^{[2]}(\epsilon,\epsilon',\gamma,\gamma')=a_5^{[2]}(\epsilon'\epsilon,\gamma',\gamma)$$
$$=2\,{\rm Im}\left[\frac{\hbar}{\epsilon_k-\epsilon-\hbar\omega_{\rm pu}+{\rm i}(\gamma_k+\gamma-\gamma_\Delta/2)}\frac{\hbar}{\epsilon_k-\epsilon'-\hbar\omega_{\rm pu}-{\rm i}(\gamma_k+\gamma'-\gamma_\Delta/2)}\right.$$
$$\times\frac{\hbar}{\epsilon_f-\epsilon-\hbar\omega_{\rm pu}-\hbar\omega_{\rm pr}+{\rm i}(\gamma-\gamma_\Delta)}\frac{\hbar}{\epsilon_f-\epsilon'-\hbar\omega_{\rm pu}-\hbar\omega_{\rm pr}-{\rm i}(\gamma'-\gamma_\Delta)}$$
$$\times\left[\frac{\hbar}{\epsilon-\epsilon'-{\rm i}(\gamma+\gamma')}+\frac{\hbar}{\epsilon_f-\epsilon-\hbar\omega_{\rm pu}-\hbar\omega_{\rm pr}+{\rm i}(\gamma+\gamma_\Delta)}\right.$$
$$\left.\left.-\frac{\hbar}{\epsilon_f-\epsilon'-\hbar\omega_{\rm pu}-\hbar\omega_{\rm pr}-{\rm i}(\gamma'+\gamma_\Delta)}-\frac{\hbar}{{\rm i}2\gamma_\Delta}\right]\right]. \tag{4.14}$$

Here, $\hat{I}^{[1]}(t_{\rm d})$ and $\hat{I}^{[2]}(t_{\rm d})$ represent the lowest and second-order terms, respectively. The first and third terms of $\hat{I}^{[1]}(t_{\rm d})$ give the IS and SS peaks, respectively, and the second term shows the interference between the processes accounting for both peaks. In $\hat{I}^{[2]}(t_{\rm d})$, the terms with coefficient $a_1^{[2]}$ give the IS peak and those with $a_4^{[2]}$ and $a_5^{[2]}$ give both the IS and SS peaks. The terms proportional to $a_2^{[2]}$ and $a_3^{[2]}$ show the interference between the processes accounting for both peaks. When γ_Δ is much smaller than the electron and hole linewidths, the terms providing no information on the lifetimes in time domain (i.e., with coefficients $a_3^{[1]}$, $a_4^{[2]}$ and $a_5^{[2]}$) become dominant (the spectrum obtained is not exactly identical to (3.1) for continuous light since the envelope function of the pulse becomes a step function here). This means that the processes which become available due to the uncertainty between time and energy provide information on the lifetimes in the analyses in the time domain so that T_1 and T_2 can be obtained as different values for TR- and ER-2PPE spectroscopy.

On comparison with the macroscopic theory (see the appendix), the non-interference terms suggest the relation of $\Gamma_1 \sim \gamma_k+\gamma_q$ or $\Gamma_1 \sim \gamma_k+\gamma$, where γ denotes the total linewidth of the secondary electrons and holes. On the other hand, the interference terms rather suggest $\Gamma_1+\Gamma_2 \sim \gamma_k+\gamma_q$ or $\Gamma_1+\Gamma_2 \sim \gamma_k+\gamma$. In order to investigate the above relations in detail, a numerical analysis is made by giving $\mathcal{E}(t)={\rm sech}(a_t t/t_\Delta)$, where $a_t=1.76$ and $t_\Delta=60$ fs (full width at half-maximum). Figure 5 shows the TR-2PPE spectrum of Cu(111) obtained. The photon energies are given by $\hbar\omega_{\rm pu}=\epsilon_k-\epsilon_q-0.10\,{\rm eV}=4.47\,{\rm eV}$ and $\hbar\omega_{\rm pr}=2.00\,{\rm eV}$ so that the energy spectrum at each $t_{\rm d}$ exhibits a two-peak structure. When the shifts due to interference are ignored, the energy positions of the peaks are estimated from $\epsilon_q+\hbar\omega_{\rm pu}+\hbar\omega_{\rm pr}=6.02\,{\rm eV}$ for the SS peak and $\epsilon_k+\hbar\omega_{\rm pr}=6.12\,{\rm eV}$ for the IS peak. Pump–probe correlation traces at these energy positions are shown in figure 6. In the process accounting for the SS peak, the

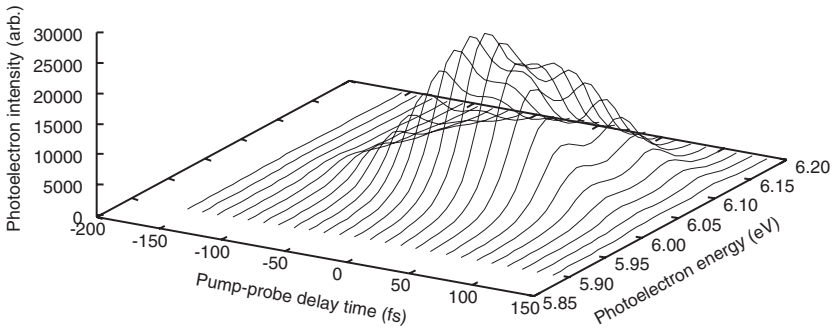

Figure 5. The TR-2PPE spectrum of Cu(111) obtained from the microscopic theory. The origin of the photoelectron energy is the Fermi level. The pulse envelope function is of sech^2 type.

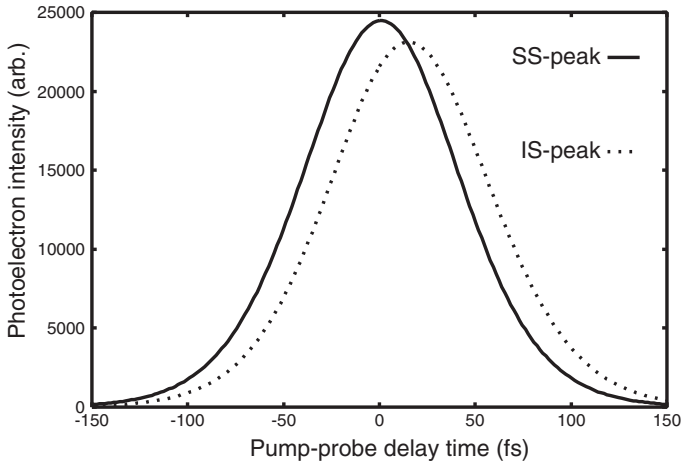

Figure 6. Pump–probe cross-correlation traces at the SS and IS peaks in the TR-2PPE spectrum of Cu(111) obtained from the results shown in figure 5.

intermediate state is a virtual state which vanishes rapidly so that the correlation trace becomes nearly a direct correlation between the pump and probe pulses and hence the maximum of the trace is fixed at $t_\mathrm{d} = 0$. The width of the trace can decrease due to the dephasing. When fitting the results with the macroscopic theory for free parameters T_1 and T_2 to figure 6 by the least squares method, the fitting succeeds very well for $T_2 = 23.4$ fs so that the fitting errors are too small to show. Here, it is noted that $T_1 = 20.5$ fs is obtained by this fitting; however, it will have no physical meaning because the trace at the SS peak is little affected by T_1.

In the process accounting for the IS peak, the intermediate state is a real state which has a finite lifetime accounting for the shift of the maximum of the correlation trace. In the macroscopic theory, the shift of the maximum is mainly determined by t_Δ and T_1, and the width of this trace is affected by both T_1 and T_2. In the same way as for the SS peak, the fitting of the results with the macroscopic theory to the trace at the IS peak position succeeds very well for parameters $T_1 = 9.6$ fs and $T_2 = 22.6$ fs. T_1 is near $[\tau_k^{-1} + \tau_q^{-1}]^{-1} = 12$ fs and smaller than the effective value of $[\tau_k^{-1} + \hbar/2\gamma]^{-1} \simeq \tau_k$ expected from figure 4. This shows that the energy relaxation at the surface corresponds to the energy dissipation due to the decay of the polarization consisting of $|q\rangle$ and $|k\rangle$ rather than the decay of the single electron in $|k\rangle$.

For both the IS and SS peak positions, the T_2 obtained is near τ_q (confirmed by calculations for various τ_k and τ_q) so that the relation of the hole decay and dephasing can be shown in the same way as the analysis of the ER-2PPE spectra. However, this relation is still not quantitatively evident since the analytically expected value of T_2, i.e., $2[\tau_k^{-1} + \tau_q^{-1} - T_1^{-1}]^{-1}$ or $2[\tau_k^{-1} + \hbar/2\gamma - T_1^{-1}]^{-1}$, becomes negative on using the T_1 obtained. Thus it is considered that the fitting for T_2 is subtle work, since the contribution from the interference terms which contain the information on the dephasing is minor compared with that of the non-interference terms.

5. Summary

Electronic relaxation in two-photon photoemission from Cu(111) was investigated from the viewpoint of many-body dynamics. The relations of the macroscopic relaxation times with the microscopic electron and hole lifetimes are clarified by analysis of the energy spectra for continuous light and the time-resolved spectra for femtosecond laser pulses. Inelastic scattering of holes which are excited into the occupied surface states by the pump laser accounts for the macroscopic dephasing, and accelerates the energy relaxation due to inelastic scattering of electrons photoexcited into the unoccupied states. T_1 and T_2 can be obtained as different values from the analyses in time and energy domains, since in the analysis in the time domain the information on T_1 and T_2 is provided by processes which become available for short laser pulses due to the uncertainty between time and energy. Concerning the energy relaxation, $\Gamma_1 = \hbar/2T_1$ is shown to depend on the detuning from the analysis of the energy spectra, and $T_1 \simeq [\tau_k^{-1} + \tau_q^{-1}]^{-1}$ ($\Gamma_1 \simeq \gamma_k + \gamma_q$) is obtained from the analysis of the time-resolved spectra for -100 meV detuning. Meanwhile, concerning the dephasing, the relation $\Gamma_2 = \gamma_q$ ($T_2 = 2\tau_q$) is clearly demonstrated both analytically and numerically from the analysis of the energy spectra whereas $T_2 \sim \tau_q$ is obtained numerically from the analysis the time-resolved spectra although the relation is still not quantitatively evident from the analytical consideration. For more detailed comparison between the energy- and time-resolved spectra, investigation of the detuning dependence of the time-resolved spectra will be required as future subjects. For comparison with experiments, accumulation of experimental data on T_1 and T_2 as functions of detuning is looked forward to.

Acknowledgments

This work was based on research in Osaka university and RIKEN. The author acknowledges Professor Hideaki Kasai and Professor Toshiaki Munakata for providing the opportunities for the research and valuable discussions.

Appendix. TR-2PPE spectra from the macroscopic theory

In order to investigate the relation with the microscopic theory in section 4, we derive the formula for the TR-2PPE spectra from the macroscopic theory usually used in the analysis of the experimental data. On the basis of the density matrix method, we introduce a model of 2PPE from an open two-level system consisting of an occupied state $|0\rangle$ and an unoccupied state $|1\rangle$ at the surface to a final state $|2\rangle$. We give the unperturbed Hamiltonian as

$$H_{0\,mm}^{\mathrm{macro}} = \delta_{mn}\epsilon_m \qquad (m, n = 0, 1, 2), \tag{A.1}$$

and the interactions with the laser pulses as

$$W_{10}^{\mathrm{macro}}(t) = [W_{01}^{\mathrm{macro}}(t)]^* = -M_{10}\mathcal{E}(t)\mathrm{e}^{\mathrm{i}\omega_{\mathrm{pu}}t}, \tag{A.2}$$

$$W_{21}^{\rm macro}(t;t_{\rm d}) = [W_{12}^{\rm macro}(t;t_{\rm d})]^* = -M_{21}\mathcal{E}(t-t_{\rm d})\mathrm{e}^{\mathrm{i}\omega_{\rm pr}t}. \tag{A.3}$$

Then, within the fourth order with respect to $W^{\rm macro}$, we solve a set of simultaneous equations:

$$\mathrm{i}\hbar\frac{\partial\rho_{mn}^{\rm macro}(t;t_{\rm d})}{\partial t} = [H_0^{\rm macro} + W^{\rm macro}(t),\, \rho^{\rm macro}(t;t_{\rm d})]_{mn} - \mathrm{i}\Gamma_{mn}\rho_{mn}^{\rm macro}(t;t_{\rm d}), \tag{A.4}$$

$$\rho_{00}^{\rm macro}(t;t_{\rm d}) \simeq 1, \tag{A.5}$$

where $m, n = 0, 1, 2$ except for $m = n = 0$. Here the density matrix $\rho^{\rm macro}(t;t_{\rm d})$ is defined in the Schrödinger representation. The diagonal elements of Γ are given by $\Gamma_{22} \to 0$ and $\Gamma_{11} = 2\Gamma_1$. The off-diagonal elements are given by $\Gamma_{12} = \Gamma_{21} = \Gamma_1$, $\Gamma_{01} = \Gamma_{10} = \Gamma_1 + \Gamma_2$ and $\Gamma_{02} = \Gamma_{20} = \Gamma_2$. Then we obtain the density of $|2\rangle$ by calculating $\rho_{01}^{\rm macro} = [\rho_{10}^{\rm macro}]^*$, $\rho_{11}^{\rm macro}$, $\rho_{02}^{\rm macro} = [\rho_{20}^{\rm macro}]^*$, $\rho_{12}^{\rm macro} = [\rho_{21}^{\rm macro}]^*$ and $\rho_{22}^{\rm macro}$ in order.

Unlike in the microscopic theory in which the hole decay results in density decay of the final state of the system as discussed in section 2, it is assumed in the macroscopic theory that the photoelectron intensity is proportional to $\rho_{22}^{\rm macro}(t)$ at $t \to \infty$ since the lifetime of the final state is given as infinite. Then, for exponential pulses given by $\mathcal{E}(t) = \bar{\mathcal{E}}\theta(t)\exp(-\gamma_\Delta t/2\hbar)$, the photoelectron intensity is obtained as

$$\begin{aligned} I^{\rm macro}(t_{\rm d}) &\propto \lim_{t\to\infty}\rho_{22}^{\rm macro}(t;t_{\rm d}) \\ &= |M_{21}M_{10}|^2|\bar{\mathcal{E}}|^4\big[A_1\theta(t_{\rm d})[\mathrm{e}^{-2\Gamma_1 t_{\rm d}/\hbar} - \mathrm{e}^{-\gamma_\Delta t_{\rm d}/\hbar}] \\ &\quad - \mathrm{Re}[A_2\theta(t_{\rm d})[\mathrm{e}^{[\mathrm{i}(\epsilon_1-\epsilon_0-\hbar\omega_{\rm pu})-\Gamma_1-\Gamma_2-\gamma_\Delta/2]t_{\rm d}/\hbar} - \mathrm{e}^{-\gamma_\Delta t_{\rm d}/\hbar}]] \\ &\quad + A_3[\theta(t_{\rm d})\mathrm{e}^{-\gamma_\Delta t_{\rm d}/\hbar} + \theta(-t_{\rm d})\mathrm{e}^{\gamma_\Delta t_{\rm d}/\hbar}]\big], \end{aligned} \tag{A.6}$$

$$\begin{aligned} A_1 = \mathrm{Re}\Bigg[&\frac{\hbar^2}{(\epsilon_2-\epsilon_1-\hbar\omega_{\rm pr})^2 + (\Gamma_1+\gamma_\Delta/2)^2} \\ &\times \frac{\hbar}{\epsilon_1-\epsilon_0-\hbar\omega_{\rm pu}-\mathrm{i}(\Gamma_1-\Gamma_2-\gamma_\Delta/2)}\frac{\hbar}{\mathrm{i}(2\Gamma_1+\gamma_\Delta)}\Bigg], \end{aligned} \tag{A.7}$$

$$\begin{aligned} A_2 = &\frac{\hbar}{\epsilon_2-\epsilon_1-\hbar\omega_{\rm pr}-\mathrm{i}(\Gamma_1+\gamma_\Delta/2)}\frac{\hbar}{\epsilon_2-\epsilon_0-\hbar\omega_{\rm pu}-\hbar\omega_{\rm pr}+\mathrm{i}(\Gamma_2+\gamma_\Delta)} \\ &\times \frac{\hbar}{\epsilon_1-\epsilon_0-\hbar\omega_{\rm pu}-\mathrm{i}(\Gamma_1-\Gamma_2-\gamma_\Delta/2)} \\ &\times \frac{\hbar}{\epsilon_1-\epsilon_0-\hbar\omega_{\rm pu}+\mathrm{i}(\Gamma_1+\Gamma_2-\gamma_\Delta/2)}, \end{aligned} \tag{A.8}$$

$$\begin{aligned} A_3 = \mathrm{Re}\Bigg[&\Bigg[\frac{\hbar}{\epsilon_2-\epsilon_0-\hbar\omega_{\rm pu}-\hbar\omega_{\rm pr}+\mathrm{i}(\Gamma_2+\gamma_\Delta)} - \frac{\hbar}{\epsilon_2-\epsilon_1-\hbar\omega_{\rm pr}+\mathrm{i}(\Gamma_1+\gamma_\Delta/2)}\Bigg] \\ &\times \Bigg[\frac{\hbar}{\epsilon_2-\epsilon_1-\hbar\omega_{\rm pr}-\mathrm{i}(\Gamma_1+\gamma_\Delta/2)} + \frac{\hbar}{\mathrm{i}2\gamma_\Delta}\Bigg]\frac{\hbar}{\epsilon_2-\epsilon_1-\hbar\omega_{\rm pr}-\mathrm{i}(\Gamma_1-3\gamma_\Delta/2)} \\ &\times \frac{\hbar}{\epsilon_1-\epsilon_0-\hbar\omega_{\rm pu}-\mathrm{i}(\Gamma_1-\Gamma_2-\gamma\Delta/2)}\Bigg]. \end{aligned} \tag{A.9}$$

The first term of $I^{\rm macro}(t_{\rm d})$ gives the IS peak and its decay rate in the time domain reflects Γ_1. The second term shows the interference between the processes accounting for the IS and SS peaks and its decay rate reflects both Γ_1 and Γ_2. The third term gives the base shape of the pump–probe correlation traces at both the IS and SS peaks, reflecting the envelope function of the input laser pulses. In the same way as in the microscopic theory, the terms proportional to $\theta(t_{\rm d})\mathrm{e}^{-\gamma_\Delta t_{\rm d}/\hbar} + \theta(-t_{\rm d})\mathrm{e}^{\gamma_\Delta t_{\rm d}/\hbar}$ become dominant when $\gamma_\Delta \ll \Gamma_1, \Gamma_2$.

References

[1] Loudon R 1983 *The Quantum Theory of Light* 2nd edn (New York: Oxford University Press)
[2] Abelés E (ed) 1972 *Optical Properties of Solids* (Amsterdam: North-Holland)
[3] Wolf M, Knoesel E and Hertel T 1996 *Phys. Rev.* B **54** R5295
[4] Wolf M, Hotzel A, Knoesel E and Velic D 1999 *Phys. Rev.* B **59** 5926
[5] Miller A D, Bezel I, Gaffney K J, Garrett-Roe S, Liu S H, Szymanski P and Harris C B 2002 *Science* **297** 1163
[6] Hotzel A, Moos G, Ishioka K, Wolf M and Ertl G 1999 *Appl. Phys.* B **68** 615
[7] Link S, Dürr H A, Bihlmayer G, Blügel S, Eberhardt W, Chulkov E V, Silkin V M and Echenique P M 2001 *Phys. Rev.* B **63** 115420
[8] Link S, Sievers J, Dürr H A and Eberhardt W 2001 *J. Electron Spectrosc. Relat. Phenom.* **114–116** 351
[9] Fauster T 2002 *Surf. Sci.* **507–510** 256
[10] Höfer U 1999 *Appl. Phys.* B **68** 383
[11] Steinmann W 1989 *Appl. Phys.* A **49** 365
[12] Davison S G and Stęślicka M 1992 *Basic Theory of Surface States* (New York: Oxford Science)
[13] Ueba H and Mii T 2000 *Appl. Phys.* A **71** 537
[14] Boger K, Roth M, Weinelt M and Fauster T 2002 *Phys. Rev.* B **65** 075104
[15] Pawlik S, Bauer M and Aeschlimann M 1997 *Surf. Sci.* **377–379** 206
[16] Cao J, Gao Y, Miller R J D, Elsayed-Ali H E and Mantell D A 1997 *Phys. Rev.* B **56** 1099
[17] Knoesel E, Hotzel A and Wolf M 1998 *Phys. Rev.* B **57** 12812
[18] Sakaue M, Kasai H and Okiji A 2001 *Appl. Surf. Sci.* **169/170** 68
[19] Sakaue M, Kasai H and Okiji A 2000 *J. Phys. Soc. Japan* **69** 160
[20] Kasai H, Diño W A and Okiji A 2001 *Surf. Sci. Rep.* **43** 1
[21] Knorren R, Bennemann K H, Burgermeister R and Aeschlimann M 2000 *Phys. Rev.* B **61** 9427
[22] Aeschlimann M, Bauer M, Paulik S, Knorren R, Bouzerar G and Bennemann K H 2000 *Appl. Phys.* A **71** 485
[23] Petek H, Nagano H, Weida M J and Ogawa S 2000 *Chem. Phys.* **251** 71
[24] Sakaue M, Munakata T, Kasai H and Okiji A 2003 *Surf. Sci.* **532–535** 30
[25] Sakaue M, Munakata T, Kasai H and Okiji A 2002 *Phys. Rev.* B **66** 094302
[26] Sakaue M, Munakata T, Kasai H and Okiji A 2003 *Phys. Rev.* B **68** 205421
[27] Echenique P M, Osma J, Machado J, Silkin V M, Chulkov E V and Pitarke J M 2001 *Prog. Surf. Sci.* **67** 271
[28] Chulkov E V, Silkin V M and Machado M 2001 *Surf. Sci.* **482–485** 693
[29] Petek H and Ogawa S 1997 *Prog. Surf. Sci.* **56** 239
[30] Sakaue M, Munakata T, Kasai H and Okiji A 2003 *J. Vac. Soc. Japan* **46** 181 (in Japanese)
[31] Sakaue M, Kasai H and Okiji A 1999 *J. Phys. Soc. Japan* **68** 720
[32] Abrikosov A A, Gor'kov L P and Dzyaloshinskii I Ye 1965 *Quantum Field Theoretical Methods in Statistical Physics* (New York: Pergamon)
[33] Ueba H 1995 *Surf. Sci.* **334** L719
[34] Wallauer W and Fauster T 1997 *Surf. Sci.* **374** 44